IEEE Access
Multidisciplinary | Rapid Review | Open Access Journal

Received March 11, 2020, accepted March 23, 2020, date of publication April 2, 2020, date of current version April 17, 2020.

Digital Object Identifier 10.1109/ACCESS.2020.2985053

Data Fusion of UWB and IMU Based on Unscented Kalman Filter for Indoor Localization of Quadrotor UAV

WEIDE YOU[1], FANBIAO LI[1], (Member, IEEE), LIQING LIAO[1], AND MEILI HUANG[2]
[1]School of Automation, Central South University, Changsha 410083, China
[2]Beijing Institute of Spacecraft System Engineering, Beijing 100094, China

Corresponding author: Liqing Liao (zdh-dqkz@csu.edu.cn)

This work was supported in part by the National Natural Science Foundation of China under Grant 61973319, Grant 61603417, and Grant 61790571, in part by the Funds for International Cooperation and Exchange of the National Natural Science Foundation of China under Grant 61860206014, in part by the Innovation-Driven Plan in Central South University under Grant 2017CX005, and in part by the 111 Project of China under Grant B17048.

ABSTRACT The indoor location technique plays a essential role during the application of quadrotor unmanned aerial vehicle (UAV). However, the control design problem for the quadrotor UAV is quite difficult in the indoor environment due to the weak GPS signal. Based on Ultra Wide Band (UWB), the related positioning issues can be solved of UAV through base station with known coordinate position and equipment with location tag, but it is difficult to meet the high-precision operation requirements. In this paper, an indoor positioning design method combined with the Inertial Measurement Unit (IMU) and UWB positioning technology is proposed, which can effectively suppress the error accumulation of the IMU and further improve the positioning accuracy. Moreover, the system architecture for a class of quadrotor UAV is designed. The multisensor fusion technology based on unscented Kalman filter (UKF) is used to avoid neglecting the high-order terms of the nonlinear observation equations of UWB and IMU, which can effectively improve the accuracy of solving the nonlinear equations. Finally, a hardware-in-the-loop simulation platform is designed to verify the effectiveness of the indoor positioning method and improve the positioning accuracy.

INDEX TERMS Ultra wide band (UWB), inertial measurement unit (IMU), data fusion, indoor localization, quadrotor UAV.

I. INTRODUCTION

The quadrotor UAV, base on the outdoor positioning technology, has been widely used in military, industrial, agricultural, entertainment and other aspects [1], for instance, air reconnaissance UAV [2], electric patrol UAV [3], [4], plant protection UAV [5], and aerial photography UAV [6]–[8], etc. However, due to the weak indoor GPS signal or no GPS signal, the positioning accuracy is directly affected, which brings limitations to the application of four rotor UAV Based on indoor positioning technology. In recent years, the industry has a great demand for UAV inspection based on indoor positioning technology, and the related control optimization, path tracking and other issues have received increasing attention.

The associate editor coordinating the review of this manuscript and approving it for publication was Fangfei Li.

It is well know that common indoor positioning schemes include vision, lidar, UWB and IMU. The motion capture system (MCS), as a kind of vision system arranged in a specific space, captures the target in the space through multiple high-speed cameras, thereby obtain the relative position of the target in the space. The positioning accuracy of the MCS can reach millimeter level, such as VICON and OptiTrack. However, it is difficult to use the MCS in some large scene areas due to the complex layout and difficult calibration. Therefore, some simultaneous localization and mapping (SLAM) schemes have emerged, such as Oriented FAST and Rotated BRIEF SLAM (ORB-SLAM) [9], semi-direct visual odometry (SVO) [10], direct sparse odometry (DSO) [11], which use a single monocular camera or a binocular camera placed on the UAV body to get the relative position of the UAV in the environment. SLAM relies on the richness of lighting and environment texture, however, most indoor

environments are not rich in texture, which will affect the accuracy and reliability of the positioning scheme. In addition, there are some positioning schemes based on lidar, such as Gmapping [12], Hector [13], Cartographer [14]. The lidar applied to the quadrotor UAV is generally a single-line lidar due to its large weight, which can only obtain the two-dimensional position of the UAV, so its altitude information cannot be obtained. UWB [15], [16] positioning scheme is light in weight, simple in layout, stable in positioning and the accuracy can reach to less than ten centimeter. It should be pointed that the positioning accuracy of UWB separate cannot meet the requirements of indoor high-precision operation. IMU is a common sensor for robot pose estimation, which has the advantages of high accuracy, fast update frequency and small size. However, IMU estimates its position by integration, and there will be accumulated errors. In addition, the position estimation will drift after a long time operation. The advantages of UWB and IMU can be obtained by integrating them. On the one hand, IMU improves the positioning accuracy. On the other hand, UWB can suppress the integral divergence of IMU and make the position estimation continue. Although the 3D position estimation is obtained in reference [17], there is still an accuracy greater than 20cm, because it has not been fused with IMU. In reference [18], UWB and IMU are fused to get 2D position estimation of the car with higher accuracy. In reference [19], the fusion of UWB and IMU is used to get a more accurate pedestrian pose estimation.

Common multisensor fusion algorithms include extended Kalman filter (EKF) [20], [21], unscented Kalman filter (UKF) [22], [23] and particle filter (PF) [24], etc. UWB positioning system model and IMU model are both nonlinear Gaussian models. Although extended Kalman filter and unscented Kalman filter can deal with the nonlinear Gaussian model, but they have different estimation accuracy. It has been reported in [25]–[28] that the accuracy of fusion based on Unscented Kalman filter is higher than that based on extended Kalman filter. This is because they have different ways of dealing with nonlinear models. The extended Kalman filter is a Taylor expansion of the nonlinear function around the filter value and the elimination of the second order and above term.s are eliminated. When the nonlinear degree of the system model is very high, the extended Kalman filter will have errors that cannot be ignored, and it will difficult to accurately estimate the state of the target. Unlike the extended Kalman filter, the unscented Kalman filter [29] is used to determine the sampling point near the estimation point instead of making linear approximation to the nonlinear equation at the estimation point [30], [31]. Therefore, when estimating the state of a nonlinear model, the accuracy of the unscented Kalman filter is higher than that of the extended Kalman filter. In addition, the algorithm is easy to implement, and the calculation amount is equivalent to that of the extended Kalman filter.

In view of the above discussion, there are still a series of difficult problems to be solved in the application of vision and lidar positioning scheme in quadrotor UAV, such as the strong dependence of vision positioning on the environment, the large weight of lidar, and the single line lidar can only get two-dimensional position information. Therefore, this paper considers the information fusion conceptual design of UWB and IMU. The target is predicted by IMU, and the accumulated error caused by IMU integration is suppressed by UWB positioning system with aim to get high-precision position estimation. Moreover, the design method of UWB data and IMU data fusion based on unscented Kalman filter is proposed to obtain the position information of indoor quadrotor. The simulation results show that the location accuracy of fusion design method presented in this paper is higher during the quadrotor UAV path planning.

II. SYSTEM MODELING

In this paper, the unscented Kalman filter is during the information fusion. Aiming at the motion model, the IMU is used to predict and get more accurate positioning information. For the observation model, the UWB positioning system is updated to get the final positioning information.

In order to facilitate interpretation, UWB positioning system is described first. Then, the motion model is introduced. Finally, the observation model is introduced.

The UWB positioning system used in this paper is composed of four base stations and a label. The hardware composition of the base station module and the label module is the same, but the software configuration is different. Each module mainly consists of dwm1000 chip of decawave company and STM32 single chip of ST company. The function of dwm1000 is to obtain the distance between label and base station based on the time of fly. Refer to [32], [33] for specific ranging principle.

Single chip microcomputer is used for data processing. The positioning principle of the system is to obtain the distance information from the tag to the four base stations and the distance between the base stations, then calculate the location of the tag relative to the positioning system through the geometric relationship.

Establish the UWB positioning system as shown in Figure 1 in the laboratory environment.

In Figure 1, A_0, A_1, A_2 and A_3 represent the base station, T represents the tag, and the tag is placed on the UAV. $L_{0,1}$, $L_{0,2}$, $L_{0,3}$ respectively represent the distance between base station A_0 and the other three base stations. $D_{T,0}$, $D_{T,1}$, $D_{T,2}$, $D_{T,3}$ represent the distance from the label to the four base stations respectively.

In particular, the other straight lines $\overline{A_0A_1}$, $\overline{A_0A_2}$, $\overline{A_0A_3}$ are perpendicular to each other, and A_0, A_1, A_2 are in the same horizontal plane, A_0 and A_3 are in the same vertical straight line.

Therefore, the coordinate system can be defined. The straight line $\overline{A_0A_1}$, $\overline{A_0A_2}$, $\overline{A_0A_3}$ can be defined as the x, y and z coordinate axes of the positioning system respectively, and is the origin of the coordinate system. According to the

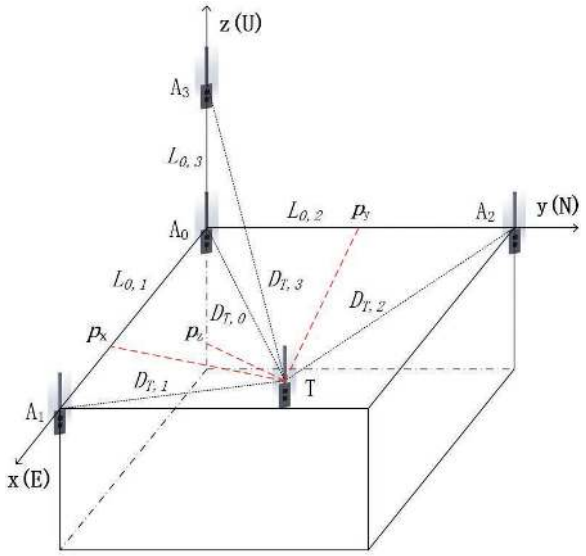

FIGURE 1. UWB positioning system. The unit of coordinate axis in the figure is meter.

right-hand rule, we arrange the coordinate system in the form of ENU (East, north, and Upward).

The direction of A_0 to A_1 is East, and it is the positive direction of x axis. The direction that A_0 points to A_2 is the north direction, which is the positive direction of the y axis. The direction A_0 points to A_3 is the upward (sky) direction, that is, the positive direction of z axis.In this paper, the UWB coordinate system arranged as above is called the world coordinate system.The intersection of the three lines is the origin of the world coordinate system, which is A_0.

In order to obtain the relationship between the coordinates of the four rotor UAV and the distance from the tag to the base station, a vertical line is made from the point T to the straight line $\overline{A_0A_1}$, $\overline{A_0A_2}$, $\overline{A_0A_3}$ and the corresponding intersection point is the coordinate value of the UAV in the world coordinate system (p_x, p_y, p_z).

So far, we have finished the introduction of the UWB positioning system. Next, we will introduce the motion model.

Due to the unscented Kalman filter has Markov property, the state prediction part is only related to the updated states and current input at the last moment, and the current input is the measurement data of acceleration and angular velocity of IMU. Define the state vector as

$$\mathbf{X} = [\mathbf{p}^{(w)}, \mathbf{v}^{(w)}, \mathbf{q}^{(w)}, \mathbf{b}_a, \mathbf{b}_g]^T, \tag{1}$$

where $\mathbf{p}^{(w)} = [p_x, p_y, p_z]^T$ is the coordinate vector of x, y and z axis of UAV in the world coordinate system, $\mathbf{v}^{(w)} = [v_x, v_y, v_z]^T$is the velocity vector of x, y and z axis of UAV in the world coordinate system, $\mathbf{q}^{(w)} = [q_W, q_X, q_Y, q_Z]^T$ is the quaternion vector of UAV attitude in the world coordinate system, $\mathbf{b}_a$ is the bias vector of accelerometer, and $\mathbf{b}_g$ is the bias vector of gyroscope.

The world coordinate system here refers to the coordinate system of UWB positioning system above, which will be introduced in Fig. 1. Equation (1) derives the time as follows:

$$\begin{aligned}\dot{\mathbf{X}} &= \begin{bmatrix}\dot{\mathbf{p}}^{(w)}\\ \dot{\mathbf{v}}^{(w)}\\ \dot{\mathbf{q}}^{(w)}\\ \dot{\mathbf{b}}_a\\ \dot{\mathbf{b}}_g\end{bmatrix} = \begin{bmatrix}\mathbf{v}^{(w)}\\ \mathbf{a}^{(w)}\\ \frac{1}{2}\mathbf{q}^{(w)} \otimes \begin{bmatrix}0\\ \boldsymbol{\omega}^{(b)}\end{bmatrix}\\ \mathbf{W}_{b_a}\\ \mathbf{W}_{b_g}\end{bmatrix}\\ &= \begin{bmatrix}\mathbf{v}^{(w)}\\ \mathbf{R}_b^w(\widetilde{\mathbf{a}}^{(b)} - \mathbf{b}_a - \mathbf{n}_a)\\ \frac{1}{2}\mathbf{q}^{(w)} \otimes \begin{bmatrix}0\\ \widetilde{\boldsymbol{\omega}}^{(b)} - \mathbf{b}_g - \mathbf{n}_g\end{bmatrix}\\ \mathbf{W}_{b_a}\\ \mathbf{W}_{b_g}\end{bmatrix},\end{aligned} \tag{2}$$

where $\mathbf{a}^{(w)}$ is the acceleration of the body in the world coordinate system, $\boldsymbol{\omega}^{(b)}$ is the angular velocity vector in the body coordinate system, $\widetilde{\mathbf{a}}^{(b)}$ is the measured value vector of the accelerometer, $\widetilde{\boldsymbol{\omega}}^{(b)}$ is the measured value vector of the gyroscope, $\mathbf{g}^{(w)} = [0, 0, -9.8]^T$ is the gravitational acceleration vector, in the coordinate system defined by UWB. $\mathbf{W}_{b_a} = \mathbf{n}_a$ and $\mathbf{W}_{b_g} = \mathbf{n}_g$ are the Gaussian white noise of the accelerometer and gyroscope respectively, $\otimes$ is the quaternion multiplication [34], $\mathbf{R}_b^{(w)}$ is the rotation matrix from the body coordinate system to the world coordinate system [35], and can be calculated by (3).

$$\begin{aligned}&\mathbf{R}_b^w\\ &= \begin{bmatrix}1-2q_Y^2-2q_Z^2 & 2q_Xq_Y-2q_Wq_Z & 2q_Xq_Z+2q_Wq_Y\\ 2q_Xq_Y+2q_Wq_Z & 1-2q_X^2-2q_Z^2 & 2q_Yq_Z-2q_Wq_X\\ 2q_Xq_Z-2q_Wq_Y & 2q_Yq_Z+2q_Wq_X & 1-2q_X^2-2q_Y^2\end{bmatrix}.\end{aligned} \tag{3}$$

The recurrence formula of the state in continuous time is given by

$$\begin{aligned}\mathbf{p}_{i+1}^{(w)} &= \mathbf{p}_i^{(w)} + \mathbf{v}_i^{(w)}\Delta t_i\\ &\quad + \iint_i^{i+1}[\mathbf{R}_b^w(\widetilde{\mathbf{a}}^{(b)} - \mathbf{b}_a - \mathbf{n}_a) + \mathbf{g}^{(w)}]dt^2, \qquad (4a)\\ \mathbf{v}_{i+1}^{(w)} &= \mathbf{v}_i^{(w)}\\ &\quad + \int_i^{i+1}[\mathbf{R}_b^w(\widetilde{\mathbf{a}}^{(b)} - \mathbf{b}_a - \mathbf{n}_a) + \mathbf{g}^{(w)}]dt, \qquad (4b)\\ \mathbf{q}_{i+1}^{(w)} &= \mathbf{q}_i^{(w)} \otimes \int_i^{i+1}(\frac{1}{2}\mathbf{q}_i^{(w)} \otimes \begin{bmatrix}0\\ \widetilde{\boldsymbol{\omega}}^{(b)} - \mathbf{b}_g - \mathbf{n}_g\end{bmatrix})dt, \qquad (4c)\end{aligned}$$

where i is the ith sampling time of UWB data.

It is worth noting that the bias of accelerometers and gyroscopes changes very slowly in a short period of time, so the integration process in a short period of time considers that the bias is constant, that is,$\mathbf{W}_{b_a} = \mathbf{n}_a = \mathbf{0}$, $\mathbf{W}_{b_g} = \mathbf{n}_g = \mathbf{0}$.

The update frequency of UWB data is less than that of IMU, and there will be multiple IMU data to be sampled between the sampling times of two UWB data. Therefore, it is necessary to integrate the IMU data when forecasting, and the median integration method is adopted here.

The recurrence formula of discrete-time state obtained by means of median integration method is as follows:

$$\mathbf{p}_{j+1}^{(w)} = \mathbf{p}_j^{(w)} + \mathbf{v}_j^{(w)}\delta t + \frac{1}{2}\widetilde{\overline{\mathbf{a}}}_j(\delta t)^2. \tag{5a}$$

$$\mathbf{v}_{j+1}^{(w)} = \mathbf{v}_j^{(w)} + \widetilde{\overline{\mathbf{a}}}_j\delta t. \tag{5b}$$

$$\mathbf{q}_{j+1}^{(w)} = \mathbf{q}_j^{(w)} \otimes \begin{bmatrix} 1 \\ \frac{1}{2}\widetilde{\overline{\boldsymbol{\omega}}}_j\delta t \end{bmatrix}. \tag{5c}$$

where j is the jth sampling time of IMU, and

$$\begin{aligned}\widetilde{\overline{\mathbf{a}}}_j = \frac{1}{2}[&(\mathbf{R}_{b_j}^w(\widetilde{\mathbf{a}}_{b_j}^{(b)} - \mathbf{b}_{a_j} - \mathbf{n}_{a_j}) + \mathbf{g}^{(w)}) \\ &+(\mathbf{R}_{b_{j+1}}^w(\widetilde{\mathbf{a}}_{b_{j+1}}^{(b)} - \mathbf{b}_{a_{j+1}} - \mathbf{n}_{a_{j+1}}) + \mathbf{g}^{(w)})].\end{aligned} \tag{6a}$$

$$\widetilde{\overline{\boldsymbol{\omega}}}_j = \frac{1}{2}[\widetilde{\boldsymbol{\omega}}_j^{(b)} + \widetilde{\boldsymbol{\omega}}_{j+1}^{(b)}] - \mathbf{b}_{g_j} - \mathbf{n}_{g_j}. \tag{6b}$$

Besides, the bias $\mathbf{b}_{g_j}$, $\mathbf{b}_{a_j}$ of IMU in two UWB sampling times is considered to be constant here.

For the observation model, it can be easily obtained according to the geometric relationship from UWB positioning system showed in Fig. 1:

$$\begin{bmatrix} D_{T,0}(k) \\ D_{T,1}(k) \\ D_{T,2}(k) \\ D_{T,3}(k) \end{bmatrix} = \begin{bmatrix} \sqrt{p_x(k)^2 + p_y(k)^2 + p_z(k)^2} \\ \sqrt{(L_{0,1} - p_x(k))^2 + p_y(k)^2 + p_z(k)^2} \\ \sqrt{p_x(k)^2 + (L_{0,2} - p_y(k))^2 + p_z(k)^2} \\ \sqrt{p_x(k)^2 + p_y(k)^2 + (L_{0,3} - p_z(k))^2} \end{bmatrix} + \begin{bmatrix} n_{T,0}(k) \\ n_{T,1}(k) \\ n_{T,2}(k) \\ n_{T,3}(k) \end{bmatrix}. \tag{7}$$

where $n_{T,0}$, $n_{T,1}$, $n_{T,2}$ and $n_{T,3}$ are the measurement noises of four distances respectively.

III. UKF BASED FUSION ALGORITHM DESIGN

The following describes the implementation details and process of the algorithm. The UKF based fusion algorithm mainly includes initialization, prediction and update.

A. INITIALIZATION

In the initialization part, the state variables and covariance matrix are initialized. By (1), the state vector includes position $\mathbf{p}^{(w)}$, velocity $\mathbf{v}^{(w)}$, rotation quaternion $\mathbf{q}^{(w)}$, accelerometer bias $\mathbf{b}_a$ and gyroscope bias $\mathbf{b}_g$. In the static state, the distance from 100 groups of labels to the base station is obtained through the UWB positioning system, and the position data is calculated through the geometric relationship. The average value is taken as the initial value of $\mathbf{p}^{(w)}$.

Using Pythagorean theorem, the specific calculation formula is as follows (8):

$$\begin{cases} p_x = \sqrt{(D_{T,0})^2 - (\frac{2S_1}{L_{0,1}})^2} \\ p_y = \sqrt{(D_{T,0})^2 - (\frac{2S_2}{L_{0,2}})^2} \\ p_z = -\sqrt{(D_{T,0})^2 - (\frac{2S_3}{L_{0,3}})^2} \end{cases} \tag{8}$$

Among them, S_1, S_2 and S_3 are the areas of $\triangle A_0A_1T$, $\triangle A_0A_2T$ and $\triangle A_0A_3T$ respectively. The calculation of the area is based on Heron's formula [36]. $\mathbf{v}^{(w)}$ is initialized to zero vector at rest.

Take the data of 100 groups of accelerometers, and calculate the roll angle of the fuselage around the x-axis of the fuselage and the pitch angle of the fuselage around the y-axis of the fuselage according to formula (9) [37]:

$$\begin{cases} \theta = arcsin(\dfrac{-A_x}{\sqrt{{A_x}^2 + {A_y}^2 + {A_z}^2}}) \\ \phi = arcsin(\dfrac{-A_y}{cos\theta\sqrt{{A_x}^2 + {A_y}^2 + {A_z}^2}}) \end{cases} \tag{9}$$

In the formula, A_x, A_y and A_z are the acceleration values of the x, y and z axes of the accelerometer respectively. The yaw angle ψ of rotation around the z-axis can be calculated according to the magnetometer in flight control, and the calculation formula [38] is:

$$\psi = -arctan(\frac{H_ycos\phi - H_zsin\phi}{H_xcos\theta + H_ysin\theta sin\phi + H_zsin\theta cos\phi}). \tag{10}$$

In the above formula, H_x, H_y and H_z are the measured values of the three axes of the magnetometer respectively. Take the average values (θ_{avg}, ϕ_{avg}, ψ_{avg}) of 100 such attitude angles and convert them into quaternions.

According to the order of z-y-x rotation, the conversion formula of quaternion of attitude angle rotation is as follows (11) [39]:

$$\mathbf{q}_0^{(w)} = \begin{bmatrix} c(\frac{\phi_{avg}}{2})c(\frac{\theta_{avg}}{2})c(\frac{\psi_{avg}}{2}) + s(\frac{\phi_{avg}}{2})s(\frac{\theta_{avg}}{2})s(\frac{\psi_{avg}}{2}) \\ s(\frac{\phi_{avg}}{2})c(\frac{\theta_{avg}}{2})c(\frac{\psi_{avg}}{2}) - c(\frac{\phi_{avg}}{2})s(\frac{\theta_{avg}}{2})s(\frac{\psi_{avg}}{2}) \\ c(\frac{\phi_{avg}}{2})s(\frac{\theta_{avg}}{2})c(\frac{\psi_{avg}}{2}) + s(\frac{\phi_{avg}}{2})c(\frac{\theta_{avg}}{2})s(\frac{\psi_{avg}}{2}) \\ c(\frac{\phi_{avg}}{2})c(\frac{\theta_{avg}}{2})s(\frac{\psi_{avg}}{2}) - s(\frac{\phi_{avg}}{2})s(\frac{\theta_{avg}}{2})c(\frac{\psi_{avg}}{2}) \end{bmatrix}. \tag{11}$$

This quaternion is taken as the initial value of $\mathbf{q}^{(w)}$. For $\mathbf{b}_a$ and $\mathbf{b}_g$, it can be obtained in IV-B.2. For covariance matrix, it can be initialized as unit matrix or use the initial set of data for calculation.

B. PREDICTION

According to the unscented Kalman filter algorithm, in the prediction part, the nonlinear function needs to be linearized by unscented transformation, and then the Gaussian probability density function is transferred by the linearized model.

1) If the first frame of IMU data or the first frame of IMU data after the unscented Kalman filter update is executed, the initialized state vector and covariance matrix or the updated state vector and covariance matrix of unscented Kalman filter are first expanded to:

$$\boldsymbol{\mu}_z = \begin{bmatrix} \widehat{\mathbf{X}}_{k-1} \\ \mathbf{0}_{6\times 1} \end{bmatrix}, \tag{12}$$

$$\boldsymbol{\Sigma}_{zz} = \begin{bmatrix} \widehat{\mathbf{P}}_{k-1} & \mathbf{0} & \mathbf{0} \\ \mathbf{0} & \mathbf{Q}_a & \mathbf{0} \\ \mathbf{0} & \mathbf{0} & \mathbf{Q}_g \end{bmatrix}. \tag{13}$$

This is because the noise covariance of accelerometers and gyroscopes is also uncertain.

2) The formula (14) and (15) produce $2N + 1(N = dim(\boldsymbol{\Sigma}_{zz}) = 22)$ sigma points $\mathbf{Z}^{(n)}$ and corresponding weight $w^{(n)}$:

$$\mathbf{Z}^{(n)} = \begin{cases} \boldsymbol{\mu}_z, & n = 0 \\ \boldsymbol{\mu}_z + \mathbf{C}_n(\sqrt{(N+\lambda)\boldsymbol{\Sigma}_{zz}}), & n = 1 \sim N \\ \boldsymbol{\mu}_z - \mathbf{C}_{n-N}(\sqrt{(N+\lambda)\boldsymbol{\Sigma}_{zz}}), & n = (N+1) \sim 2N \end{cases} \tag{14}$$

$$w^{(n)} = \begin{cases} \dfrac{\lambda}{N+\lambda}, & n = 0 \\ \dfrac{1}{2(N+\lambda)}, & n = 1 \sim 2N \end{cases} \tag{15}$$

where $\mathbf{C}_n$ represents column n of matrix, the same below. N is the dimension of the expanded state vector, λ is a scaling parameter, and its setting reference [29].

3) Integrate IMU data before UWB data update.
Since the covariance matrix is expanded in (13), each sigma point in (14) is expanded into the form of state and motion noise:

$$\mathbf{Z}^{(n)} = \begin{bmatrix} \widehat{\mathbf{X}}_{k-1,n} \\ \mathbf{n}_{a,n} \\ \mathbf{n}_{g,n} \end{bmatrix}. \tag{16}$$

Then, when the IMU data is updated, each sigma point is brought into (5c) for calculation until the UWB data is updated. At this time, the state vector calculated by each sigma point is recorded as $\check{\mathbf{X}}_{k,n}$.

4) Recombine $\check{\mathbf{X}}_{k,n}$. and its corresponding weights into prediction confidence:

$$\check{\mathbf{X}}_k = \sum_{n=0}^{2N} w^{(n)} \check{\mathbf{X}}_{k,n}, \tag{17}$$

$$\check{\mathbf{P}}_k = \sum_{n=0}^{2N} w^{(n)} (\check{\mathbf{X}}_{k,n} - \check{\mathbf{X}}_k)(\check{\mathbf{X}}_{k,n} - \check{\mathbf{X}}_k)^T. \tag{18}$$

So far, we have got the mean value and variance of the prediction part, and prepared the data for the update part. Next update.

C. UPDATE

Similar to the prediction procedure, the tracking free transformation is also needed in the update part, because the observation model is also a nonlinear model.

1) The mean and covariance of the prediction are expanded to:

$$\boldsymbol{\mu}_s = \begin{bmatrix} \check{\mathbf{X}}_k \\ \mathbf{0}_{4\times 1} \end{bmatrix}, \tag{19}$$

$$\boldsymbol{\Sigma}_{ss} = \begin{bmatrix} \check{\mathbf{P}}_k & \mathbf{0} \\ \mathbf{0} & \mathbf{R}_{uwb} \end{bmatrix}. \tag{20}$$

2) Generate $2M + 1(M = dim(\boldsymbol{\Sigma}_{ss}) = 20)$ sigma points $\mathbf{Y}^{(m)}$ and corresponding weight $\rho^{(m)}$ according to (21) and (22):

$$\mathbf{Y}^{(m)} = \begin{cases} \boldsymbol{\mu}_s, & m = 0 \\ \boldsymbol{\mu}_s + \mathbf{C}_m(\sqrt{(M+\lambda)\boldsymbol{\Sigma}_{ss}}), & m = 1 \sim M \\ \boldsymbol{\mu}_s - \mathbf{C}_{m-M}(\sqrt{(M+\lambda)\boldsymbol{\Sigma}_{ss}}), & m = (M+1) \sim 2M \end{cases} \tag{21}$$

$$\rho^{(m)} = \begin{cases} \dfrac{\lambda}{M+\lambda}, & m = 0 \\ \dfrac{1}{2(M+\lambda)}, & m = 1 \sim 2M \end{cases} \tag{22}$$

3) Each sigma point is expanded into the form of state and motion noise:

$$\mathbf{Y}^{(m)} = \begin{bmatrix} \check{\mathbf{X}}_{k,m} \\ \mathbf{R}_{uwb,m} \end{bmatrix}. \tag{23}$$

In the formula,

$$\mathbf{R}_{uwb,m} = \begin{bmatrix} n_{T,0}(k,m) \\ n_{T,1}(k,m) \\ n_{T,2}(k,m) \\ n_{T,3}(k,m) \end{bmatrix}. \tag{24}$$

Then, each sigma point is carried into (7) to calculate $\mathbf{D}_{k,m}$.

4) The mean value and covariance of the observations are obtained by recombining and its corresponding weights:

$$\mathbf{D}_k = \sum_{m=0}^{2M} \rho^{(m)} \mathbf{D}_{k,m}, \tag{25}$$

$$\boldsymbol{\Sigma}_{DD} = \sum_{m=0}^{2M} \rho^{(m)} (\mathbf{D}_{k,m} - \mathbf{D}_k)(\mathbf{D}_{k,m} - \mathbf{D}_k)^T. \tag{26}$$

5) Calculate the unscented Kalman gain and update the state variables and covariance:

$$\mathbf{K}_k = \boldsymbol{\Sigma}_{XD} \boldsymbol{\Sigma}_{DD}^{-1}, \tag{27}$$

$$\widehat{\mathbf{X}}_k = \check{\mathbf{X}}_k + \mathbf{K}_k(\check{\mathbf{D}}_k - \mathbf{D}_k), \tag{28}$$

$$\widehat{\mathbf{P}}_k = \check{\mathbf{P}}_k - \mathbf{K}_k \boldsymbol{\Sigma}_{XD}^T. \tag{29}$$

where $\check{\mathbf{D}}_k$ is the distance vector from the label to the base station in the UWB positioning system, and

$$\mathbf{\Sigma}_{XD} = \sum_{m=0}^{2M} \rho^{(m)}(\check{\mathbf{X}}_{k,m} - \check{\mathbf{X}}_k)(\mathbf{D}_{k,m} - \mathbf{D}_k)^T. \quad (30)$$

Update the state vector and covariance matrix to prepare for the next iteration. This completes the update step.

D. ALGORITHM FLOW CHART

The above describes the initialization, prediction and update of the algorithm process, and the following describes the specific operation process of the algorithm. Since the update frequency of IMU is faster than that of UWB, the data of IMU is integrated between two frames of UWB data, and the result of integration is used as the prediction of Unscented Kalman filter.

When UWB data is updated, unscented Kalman filter is updated. Fig. 2 is the time flow chart of IMU and UWB data fusion.

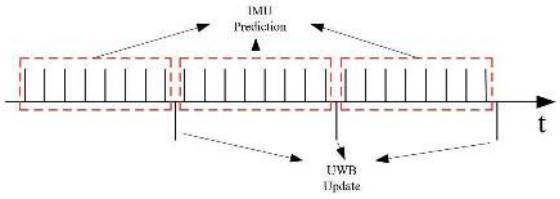

FIGURE 2. Time flow chart of data fusion between IMU and UWB.

Fig. 3 is the algorithm operation flow chart. At the beginning of the algorithm, initialization of relevant variables and parameters is carried out first, followed by data fusion process, that is, repeated prediction and update. In Fig. 3, the red virtual border part is the prediction part, and the green virtual border part is the update part.

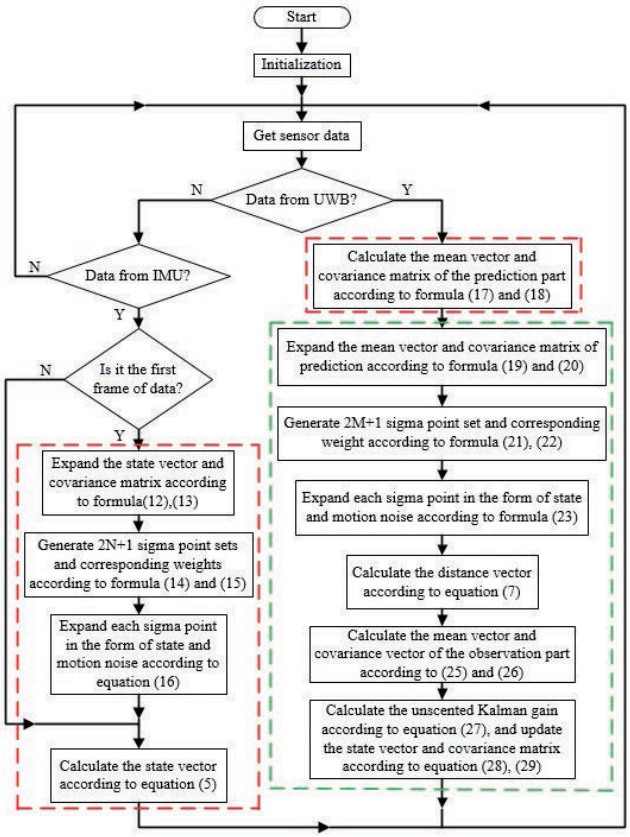

FIGURE 3. Algorithm operation flow chart.

IV. EXPERIMENTAL PLATFORM AND SIMULATIONS

This part is the experimental part. Firstly, it introduces the experimental environment, including software and hardware. Secondly, it preprocesses the data before fusion, so as to carry out data fusion. Finally, it carries out data fusion experiments in the indoor environment, and analyzes the experimental results.

A. EXPERIMENTAL ENVIRONMENT

The composition of the experimental platform is shown in Fig. 4, mainly including software and hardware. The main body of the software is ROS, a small development operating system running on the Ubuntu operating system. The corresponding functions are realized by ROS nodes, such as location data acquisition, data fusion filtering and UAV position control.

The hardware mainly includes four rotor frame, airborne computer NVIDIA Jetson TX2 (hereinafter referred to as TX2), flight controller pixhawk, UWB positioning system.

FIGURE 4. Experimental platform.

Airborne computer is mainly used to run ROS, while flight controller is used to read sensor data and related control.

As shown in Fig. 5, the onboard computer TX2 can receive IMU data sent by the flight controller pixhawk, including accelerometer data and gyroscope data, through mavros (mavros is the ROS interface function package for TX2 to communicate with pixhawk).

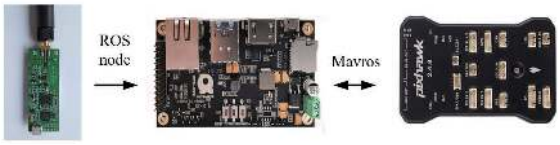

FIGURE 5. Schematic diagram of data acquisition.

In addition, the location data of UWB can be read by ROS node.

Next, preprocess the acquired data, and then carry out data fusion.

B. DATA PREPROCESSING

1) CALIBRATION OF UWB DATA

In different indoor environment, UWB often shows the phenomenon that the measured value is larger than the actual value or smaller than the actual value, so this paper does the following calibration work. A base station and a label are set in the environment to fix the base station in a position, and then the labels are moved to the preset positions with a certain distance from the base station. Read the 50 UWB distance measurements of the label at each preset position, take the average of the 50 measurements as the measurement value of the distance, record the data as shown in Table 1, and plot each actual distance value and its UWB measurement value in Fig. 6.

TABLE 1. The actual distance value and the UWB observation distance value record table.

AV	100	200	300	400	500	600	700
OM	577.83	786.41	896.54	996.46	1074.28	1212.19	1305.28
AV	800	900	1000	1100	1200	1300	1400
OM	1397.23	1478.65	1578.52	1658.44	1763.28	1878.68	1973.65
AV	1500	1600	1700	1800	1900	2000	2100
OM	2074.65	2172.19	2277.93	2380.19	2593.41	2680.48	2728.94
AV	2200	2300	2400	2500	2600	2700	2800
OM	2829.06	2942.37	3054.43	3120.69	3217.33	3330.61	3423.39

AC = actual value, the data in the same row as AC is the actual value, and its unit is millimeter.
OM = observation mean, the data in the same row as OM is the measured value, and its unit is millimeter.

It can be seen that the relationship between the observation value and the actual value is approximately linear, so the linear fitting is carried out in this paper. Take the actual value as an independent variable and the measured value as a function, use the data linear equation fitting function of Excel software to perform linear fitting, and get the relationship between the observation value and the actual value x_{ac} using $y_{ob} = ax_{ac} + b$. Then there is $x_{ac} = \frac{y_{ob}-b}{a}$, that is to say, the UWB estimate corresponding to the actual distance value can be obtained by the formula.

The above is only a linear fitting of the measurement data, considering a wide environment without obstacles. If there are obstacles between the base station and the label in the application environment, it is easy to affect the measurement accuracy of UWB. At this time, the influence of the obstacle weakening UWB signal on the measurement should be considered. For specific measures, please refer to [40]. During the use, the tag and base station should be placed vertically, and the pitch and roll angles of the four rotor UAV equipped with the tag should not be too large, otherwise the measurement accuracy will be reduced due to the too large tilt angle of the tag. If the attitude of the UAV changes greatly in the application environment, the measurement error caused by the attitude change should be compensated, refer to [41] for details. In addition, if the application scenario is complex, it is also necessary to establish an appropriate distance error calibration model for the scenario, please refer to [42].

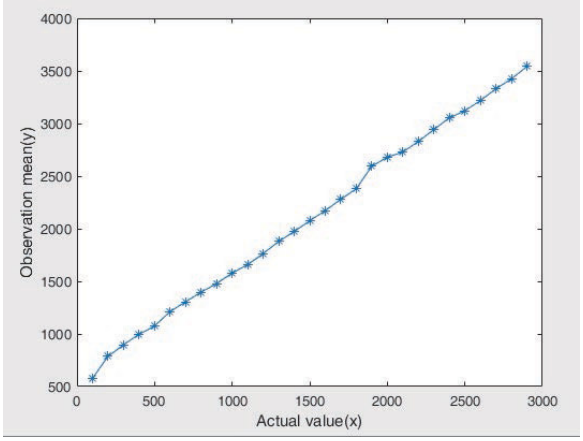

FIGURE 6. UWB data calibration results. The unit of coordinate axis in the figure is millimeter.

2) CALIBRATION OF IMU

So far, the UWB data calibration is completed. Before data fusion, the IMU in the flight controller needs to be calibrated to obtain the variance and bias information of the IMU. However, there are special software to calibrate the IMU in the flight controller, such as Allen variance curve [43], etc., so the specific calibration process will not be described here.

C. EXPERIMENT AND RESULT ANALYSIS

This experiment is carried out in an indoor environment of (3m × 2.5m × 2.4m) cubic meters, in which the positioning system as shown in Fig 1 is arranged and the label is placed on the UAV. As shown in Fig. 7, several ROS nodes are run on the on-board computer TX2 to achieve UWB data acquisition and analysis, IMU data acquisition, data fusion algorithm implementation and data recording functions.

UWB label sends data out through serial port, so this experiment uses USB to serial port module to connect the serial port of label and the USB interface of TX2 board computer, as shown in Fig. 8. Then a ROS node reading serial port is created. The node reads the UWB data and analyzes it, and gets the distance data from the tag to four base stations. Finally, the four distance data are published in the form of ROS topic, so that the ROS node that carries out data fusion and data recording receives it.

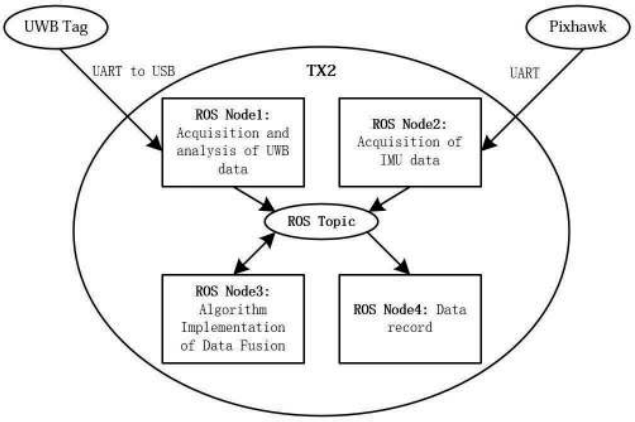

FIGURE 7. ROS node diagram.

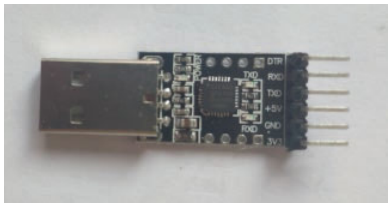

FIGURE 8. USB serial port module.

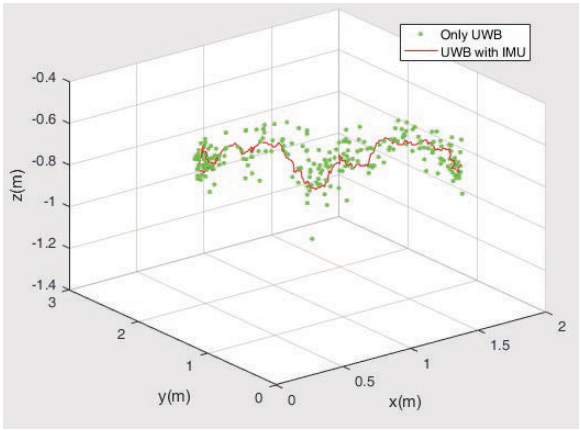

FIGURE 9. 3D positioning diagram.

IMU data comes from flight controller. TX2 onboard computer needs ROS function package named mavros to read. The specific communication protocol is mavlink. Then, the read IMU information is published in the form of ROS topic, so that the ROS node that performs data fusion receives it. The node implemented by the data fusion algorithm mainly listens to two ROS topics of UWB distance and IMU acceleration data. When any data is updated, the data fusion algorithm is executed, and the position information of the four rotors is released in the form of ROS topic, so that the ROS node recorded data can receive it. After receiving the UWB distance data, the ROS node of the data record performs the coordinate solution according to (7), and then records the coordinate data and time stamp in a file.

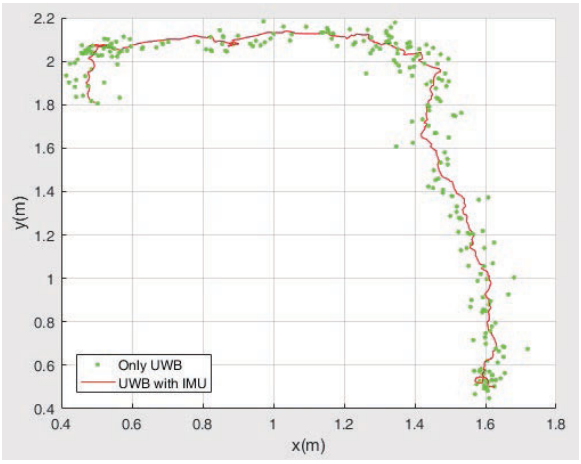

FIGURE 10. Positioning diagram of x, y plane.

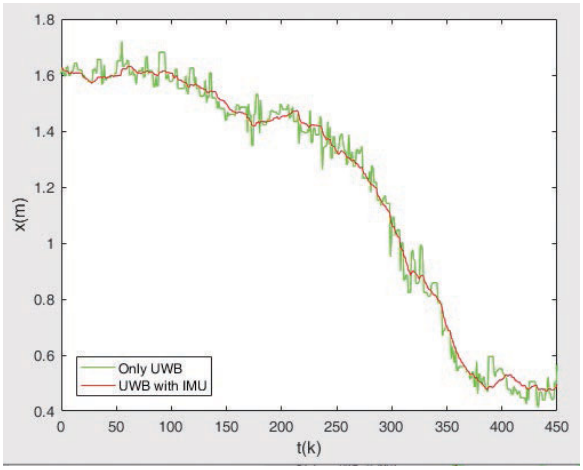

FIGURE 11. Positioning diagram x-axis.

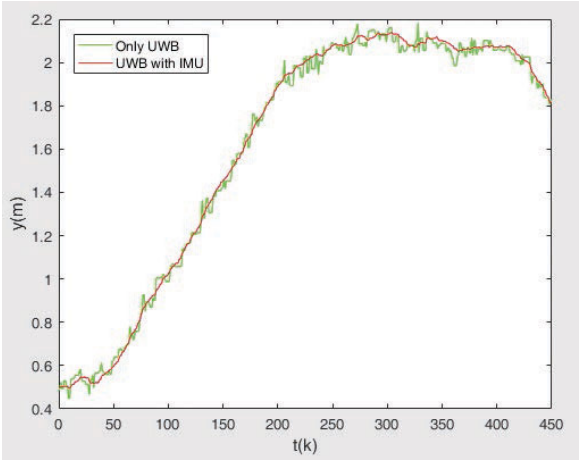

FIGURE 12. Positioning diagram of y-axis.

In addition, the ROS node of the data record also listens to the coordinate topic from the data fusion node, and records the coordinate and receiving time stamp of the topic in another file.

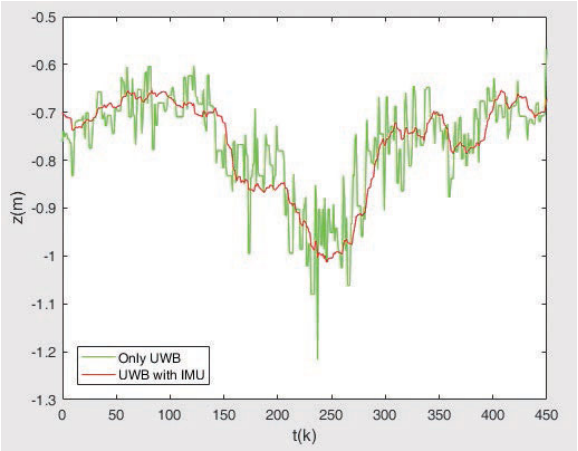

FIGURE 13. Positioning diagram of z-axis.

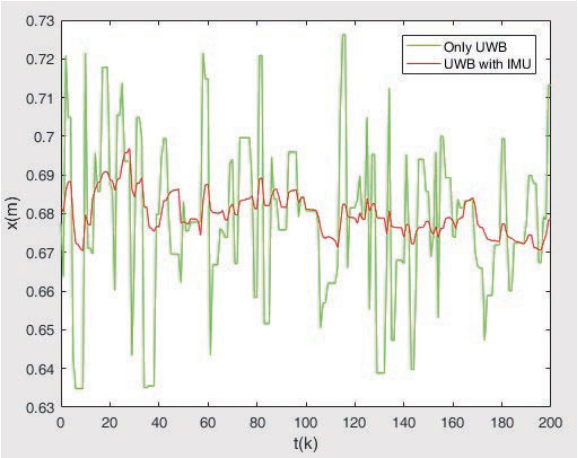

FIGURE 14. Positioning diagram of x-axis direction in static state.

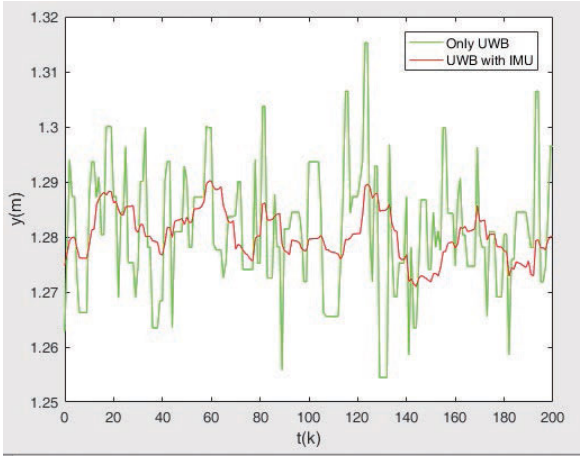

FIGURE 15. Positioning diagram of y-axis direction in static state.

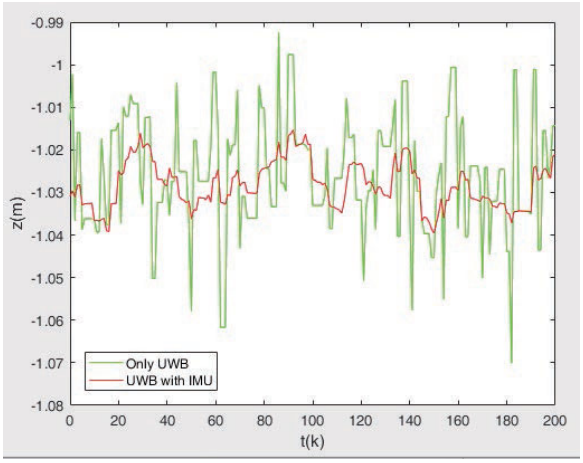

FIGURE 16. Positioning diagram of z-axis direction in static state.

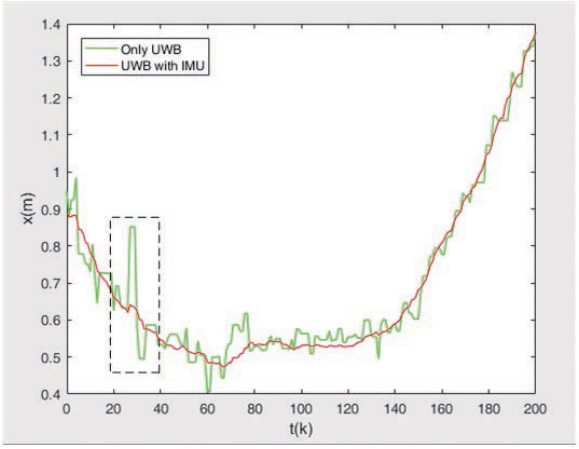

FIGURE 17. Positioning diagram of x-axis.

The above preparations for the data fusion experiment are well done. Next, the remote control four rotors fly in the built indoor environment, recording the data of UWB single positioning and the data of UWB and IMU fusion positioning. Fig. 9 is a 3D schematic diagram of UWB single positioning and UWB and IMU fusion positioning when the four rotor UAV is in indoor remote control flight, and its top view is shown in Fig. 10. By analyzing the positioning data in x, y and z directions, as shown in Fig. 11, Fig. 12 and Fig. 13, it can be seen that the accuracy of UWB and IMU fusion positioning is higher than that of UWB alone positioning.

In static state, UWB and IMU fusion positioning and UWB are waveform schematic diagrams separately located in three coordinate axes, as shown in Fig. 14, Fig. 15 and Fig. 16. It can be seen that the accuracy of UWB positioning alone is within $\pm$5cm, while the accuracy of UWB and IMU fusion positioning is within $\pm$1.5cm, and the accuracy is significantly improved.

Fig. 17 and Fig. 18 are the data waveforms of UWB single positioning and UWB and IMU fusion positioning in x-axis and y-axis collected during a remote control flight. It can be seen that when the UWB data has hourly anomalies, the data of fusion location can still ensure the correctness of the data, and the UWB anomaly has no obvious impact on the later

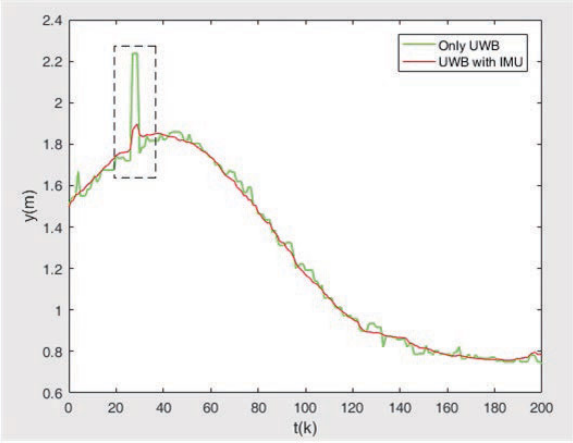

FIGURE 18. Positioning diagram y-axis.

data fusion, which is enough to show that the fusion algorithm has strong robustness.

V. CONCLUSION

In this paper, an indoor positioning design method is proposed by combining the Inertial Measurement Unit (IMU) and UWB positioning technology, which can effectively suppress the error accumulation of the IMU and further improve the positioning accuracy. The multisensor fusion technology is proposed based on unscented Kalman filter (UKF) during the path planning of quadrotor UAV, which not only improve the accuracy of positioning and enhances the robustness of positioning. Moreover, an accurate and reliable positioning scheme has been provide for indoor quadrotor UAV. Finally, a hardware-in-the-loop simulation platform is designed to verify the effectiveness of the indoor positioning method and improve the positioning accuracy.

REFERENCES

[1] K. P. Valavanis and G. J. Vachtsevanos, *UAV Applications: Introduction*. Amsterdam, The Netherlands: Springer, 2015.
[2] T. Samad, J. S. Bay, and D. Godbole, "Network-centric systems for military operations in urban Terrain: The role of UAVs," *Proc. IEEE*, vol. 95, no. 1, pp. 92–107, Jan. 2007.
[3] Z. Li, Y. Liu, R. Walker, R. Hayward, and J. Zhang, "Towards automatic power line detection for a UAV surveillance system using pulse coupled neural filter and an improved Hough transform," *Mach. Vis. Appl.*, vol. 21, no. 5, pp. 677–686, Aug. 2010.
[4] Y. Zhai, H. Zhao, M. Zhao, and S. Jiao, "Design of electric patrol UAVs based on a dual antenna system," *Energies*, vol. 11, no. 4, p. 866, 2018.
[5] Z. Yanliang, C. College of EngineeringHeilongjiang Bayi Agricultural UniversityDaqing 163319Heilongjiang, L. Qi, and Z. Wei, "Design and test of a six-rotor unmanned aerial vehicle (UAV) electrostatic spraying system for crop protection," *Int. J. Agricult. Biol. Eng.*, vol. 10, no. 6, pp. 68–76, 2017.
[6] J. C. Murray, M. J. Neal, and F. Labrosse, "Development and deployment of an intelligent kite aerial photography platform (iKAPP) for site surveying and image acquisition," *J. Field Robot.*, vol. 30, no. 2, pp. 288–307, Mar. 2013.
[7] G. Heredia, F. Caballero, I. Maza, L. Merino, A. Viguria, and A. Ollero, "Multi-unmanned aerial vehicle (UAV) cooperative fault detection employing differential global positioning (DGPS), inertial and vision sensors," *Sensors*, vol. 9, no. 9, pp. 7566–7579, 2009.
[8] A. Gurtner, D. G. Greer, R. Glassock, L. Mejias, R. A. Walker, and W. W. Boles, "Investigation of fish-eye lenses for small-UAV aerial photography," *IEEE Trans. Geosci. Remote Sens.*, vol. 47, no. 3, pp. 709–721, Mar. 2009.
[9] R. Mur-Artal and J. D. Tardos, "ORB-SLAM2: An open-source SLAM system for monocular, stereo, and RGB-D cameras," *IEEE Trans. Robot.*, vol. 33, no. 5, pp. 1255–1262, Oct. 2017.
[10] C. Forster, M. Pizzoli, and D. Scaramuzza, "SVO: Fast semi-direct monocular visual odometry," in *Proc. IEEE Int. Conf. Robot. Autom. (ICRA)*, May 2014, pp. 15–22.
[11] J. Engel, V. Koltun, and D. Cremers, "Direct sparse odometry," *IEEE Trans. Pattern Anal. Mach. Intell.*, vol. 40, no. 3, pp. 611–625, Mar. 2018.
[12] G. Grisetti, C. Stachniss, and W. Burgard, "Improved techniques for grid mapping with rao-blackwellized particle filters," *IEEE Trans. Robot.*, vol. 23, no. 1, pp. 34–46, Feb. 2007.
[13] S. Kohlbrecher, O. von Stryk, J. Meyer, and U. Klingauf, "A flexible and scalable SLAM system with full 3D motion estimation," in *Proc. IEEE Int. Symp. Saf., Secur., Rescue Robot.*, Kyoto, Japan, Nov. 2011, pp. 155–160.
[14] R. Ren, H. Fu, and M. Wu, "Large-scale outdoor SLAM based on 2D lidar," *Electronics*, vol. 8, no. 6, p. 613, 2019.
[15] G. R. Aiello and G. D. Rogerson, "Ultra-wideband wireless systems," *IEEE Microw. Mag.*, vol. 4, no. 2, pp. 36–47, Jun. 2003.
[16] A. Chehri, P. Fortier, and P. M. Tardif, "UWB-based sensor networks for localization in mining environments," *Ad Hoc Netw.*, vol. 7, no. 5, pp. 987–1000, Jul. 2009.
[17] J. Tiemann, F. Schweikowski, and C. Wietfeld, "Design of an UWB indoor-positioning system for UAV navigation in GNSS-denied environments," in *Proc. Int. Conf. Indoor Positioning Indoor Navigat. (IPIN)*, Oct. 2015, PP. 1–7.
[18] R. S. Kulikov, "Integrated UWB/IMU system for high rate indoor navigation with cm-level accuracy," in *Proc. Moscow Workshop Electron. Netw. Technol. (MWENT)*, Mar. 2018, PP. 1–4.
[19] H. Benzerrouk and A. V. Nebylov, "Robust IMU/UWB integration for indoor pedestrian navigation," in *Proc. 25th Saint Petersburg Int. Conf. Integr. Navigat. Syst. (ICINS)*, Saint Petersburg, Russia, May 2018, pp. 1–5.
[20] G. Rigatos and S. Tzafestas, "Extended Kalman filtering for fuzzy modelling and multi-sensor fusion," *Math. Comput. Model. Dyn. Syst.*, vol. 13, no. 3, pp. 251–266, Jun. 2007.
[21] A. I. Mourikis, N. Trawny, S. I. Roumeliotis, A. E. Johnson, A. Ansar, and L. Matthies, "Vision-aided inertial navigation for spacecraft entry, descent, and landing," *IEEE Trans. Robot.*, vol. 25, no. 2, pp. 264–280, Apr. 2009.
[22] X. Yuan, S. Yu, S. Zhang, G. Wang, and S. Liu, "Quaternion-based unscented Kalman filter for accurate indoor heading estimation using wearable multi-sensor system," *Sensors*, vol. 15, no. 5, pp. 10872–10890, 2015.
[23] W. Zhou and J. Hou, "A new adaptive robust unscented Kalman filter for improving the accuracy of target tracking," *IEEE Access*, vol. 7, pp. 77476–77489, 2019.
[24] S.-H.-P. Won, W. W. Melek, and F. Golnaraghi, "A Kalman/particle filter-based position and orientation estimation method using a position Sensor/Inertial measurement unit hybrid system," *IEEE Trans. Ind. Electron.*, vol. 57, no. 5, pp. 1787–1798, May 2010.
[25] S. J. Julier and J. K. Uhlmann, "A new extension of the Kalman filter to nonlinear systems," *Proc. SPIE Int. Soc. Opt. Eng.*, vol. 3068, pp. 182–193, Jun. 1999.
[26] A. Onat, "A novel and computationally efficient joint unscented Kalman filtering scheme for parameter estimation of a class of nonlinear systems," *IEEE Access*, vol. 7, pp. 31634–31655, 2019.
[27] A. Romanenko and J. A. A. M. Castro, "The unscented filter as an alternative to the EKF for nonlinear state estimation: A simulation case study," *Comput. Chem. Eng.*, vol. 28, no. 3, pp. 347–355, Mar. 2004.
[28] S. Konatowski, P. Kaniewski, and J. Matuszewski, "Comparison of estimation accuracy of EKF, UKF and PF filters," *Annu. Navigat.*, vol. 23, no. 1, pp. 69–87, Dec. 2016.
[29] L. Angrisani, M. D'Apuzzo, and R. S. Lo Moriello, "The unscented transform: A powerful tool for measurement uncertainty evaluation," *IEEE Trans. Instrum. Meas.*, vol. 55, no. 3, pp. 737–743, May 2006.
[30] W. Zhou and J. Hou, "A new adaptive high-order unscented Kalman filter for improving the accuracy and robustness of target tracking," *IEEE Access*, vol. 7, pp. 118484–118497, 2019.
[31] S. Julier, J. Uhlmann, and H. F. Durrant-Whyte, "A new method for the nonlinear transformation of means and covariances in filters and estimators," *IEEE Trans. Autom. Control*, vol. 45, no. 3, pp. 477–482, Mar. 2000.
[32] N. Patwari, J. N. Ash, S. Kyperountas, A. O. Hero, R. L. Moses, and N. S. Correal, "Locating the nodes: Cooperative localization in wireless sensor networks," *IEEE Signal Process. Mag.*, vol. 22, no. 4, pp. 54–69, Jul. 2005.

[33] Z. Sahinoglu, *Ultra-Wideband Positioning Systems*. Cambridge, U.K.: Cambridge Univ. Press, 2008.
[34] J. Sola, "Quaternion kinematics for the error-state Kalman filter," 2017, *arXiv:1711.02508*. [Online]. Available: https://arxiv.org/abs/1711.02508
[35] I. Y. Bar-Itzhack and Y. Oshman, "Attitude determination from vector observations: Quaternion estimation," *IEEE Trans. Aerosp. Electron. Syst.*, vols. AES–21, no. 1, pp. 128–136, Jan. 1985.
[36] R. C. Alperin, "Heronš area formula," *College Math. J.*, vol. 18, no. 2, pp. 137–138, 1987.
[37] Y. Liu, N. Noguchi, and K. Ishii, "Development of a low-cost IMU by using sensor fusion for attitude angle estimation," *IFAC Proc. Volumes*, vol. 47, no. 3, pp. 4435–4440, 2014.
[38] H. No, A. Cho, and C. Kee, "Attitude estimation method for small UAV under accelerative environment," *GPS Solutions*, vol. 19, no. 3, pp. 343–355, Jul. 2015.
[39] C. Zhu, J. Zhao, and Y. Liu, "Transformation between Euler angles and attitude quaternion in large angle range," *J. Chin. Inertial Technol.*, vol. 26, no. 1, pp. 115–126, 2018.
[40] C. K. Toth, G. Jozkow, Z. Koppanyi, and D. Grejner-Brzezinska, "Positioning slow-moving platforms by UWB technology in GPS-challenged areas," *J. Surveying Eng.*, vol. 143, no. 4, Nov. 2017, Art. no. 04017011.
[41] H. Perakis and V. Gikas, "Evaluation of range error calibration models for indoor UWB positioning applications," in *Proc. Int. Conf. Indoor Positioning Indoor Navigat. (IPIN)*, Nantes, France, Sep. 2018, p. 206—212.
[42] A. Ledergerber and R. D'Andrea, "Ultra-wideband range measurement model with Gaussian processes," in *Proc. IEEE Conf. Control Technol. Appl. (CCTA)*, Mauna Lani, HI, USA, Aug. 2017, pp. 1929–1934.
[43] N. El-Sheimy, H. Hou, and X. Niu, "Analysis and modeling of inertial sensors using allan variance," *IEEE Trans. Instrum. Meas.*, vol. 57, no. 1, pp. 140–149, Jan. 2008.

WEIDE YOU received the B.Sc. degree in automation from Jiangsu University, Zhenjiang, China, in 2017. He is currently pursuing the M.Sc. degree in control engineering with Central South University. His current research directions include unmanned systems and information fusion.

FANBIAO LI (Member, IEEE) received the B.Sc. degree in applied mathematics from Mudanjiang Normal University, Mudanjiang, China, in 2008, the M.Sc. degree in operational research and cybernetics from Heilongjiang University, Harbin, China, in 2012, and the Ph.D. degree in control theory and control engineering from the Harbin Institute of Technology, Harbin, in 2015.

From December 2013 to April 2015, he was a Joint Training Ph.D. Student with the School of Electrical and Electronic Engineering, The University of Adelaide, Adelaide, Australia. From April 2015 to February 2016, he was a Research Associate with the School of Electrical and Electronic Engineering, The University of Adelaide. In 2016, he joined Central South University, China, as an Associate Professor. Since April 2017, he has been an Alexander von Humboldt Research Fellow of the University of Duisburg–Essen, Duisburg, Germany. His research interests include stochastic systems, sliding mode control, and fault diagnosis and identification. He currently serves as an Associate Editor for a number of journals, including *Cognitive Computation*, IEEE Access, and *ICIC-Express Letters*. He is also an Associate Editor of the Conference Editorial Board, IEEE Control Systems Society.

LIQING LIAO received the B.Sc. degree in industrial automation, the M.Sc. degree in automation, and the Ph.D. degree in control science and engineering from Central South University, Changsha, China, in 1987, 1990, and 2010, respectively. From 1993 to 1997, he served as the Deputy Director of the Automation Teaching and Research Office, Department of Automatic Control Engineering, Central South University, where he also served as the Deputy Director and the Director of the Automation Research Institute, School of Information Science and Engineering, from 1998 to 2003. From 2003 to 2007, he served as the Deputy Director of the Department of Automation, School of Information Science and Engineering, Central South University, where he also served as the Deputy Director of the Department of Electrical Engineering, School of Information Science and Engineering, from 2007 to 2016. His current research directions are in the measurement and control technology of complex electromechanical systems.

MEILI HUANG received the B.Sc. degree in mechatronics engineering from the Beijing Institute of Technology, in 2002, and the M.Sc. degree in spacecraft design from the China Academy of Technology, in 2005. She is currently a Professor with the Beijing Institute of Spacecraft System Engineering, Beijing, China. Her research interests cover orbit dynamics and control of spacecraft.